ACS SENSORS

pubs.acs.org/acssensors
Article

Simultaneous, Real-Time Detection of Glutamate and Dopamine in Rat Striatum Using Fast-Scan Cyclic Voltammetry

Laney C. Kimble,[⊥] Jack S. Twiddy,[⊥] Jenna M. Berger, Alexandra G. Forderhase, Gregory S. McCarty, John Meitzen, and Leslie A. Sombers*

Cite This: *ACS Sens.* 2023, 8, 4091−4100
Read Online
ACCESS | Metrics & More | Article Recommendations

ABSTRACT: Glutamate and dopamine (DA) represent two key contributors to striatal functioning, a region of the brain that is essential to motor coordination and motivated behavior. While electroanalytical techniques can be utilized for rapid, spatially resolved detection of DA in the interferent-rich brain environment, glutamate, a nonelectroactive analyte, cannot be directly detected using electroanalytical techniques. However, it can be probed using enzyme-based sensors, which generate an electroactive reporter in the presence of glutamate. The vast majority of glutamate biosensors have relied on amperometric sensing, which is an inherently nonselective detection technique. This approach necessitates the use of complex and performance-limiting modifications to ensure the desired single-analyte specificity. Here, we present a novel glutamate microbiosensor fabricated on a carbon-fiber microelectrode substrate and coupled with fast-scan cyclic voltammetry (FSCV) to enable the simultaneous quantification of glutamate and DA at single recording sites in the brain, which is impossible when using typical amperometric approaches. The glutamate microbiosensors were characterized for sensitivity, stability, and selectivity by using a voltammetric waveform optimized for the simultaneous detection of both species. The applicability of these sensors for the investigation of neural circuits was validated in the rat ventral striatum. Electrically evoked glutamate and DA release were recorded at single-micrometer-scale locations before and after pharmacological manipulation of glutamatergic signaling. Our novel glutamate microbiosensor advances the state of the art by providing a powerful tool for probing coordination between these two species in a way that has previously not been possible.

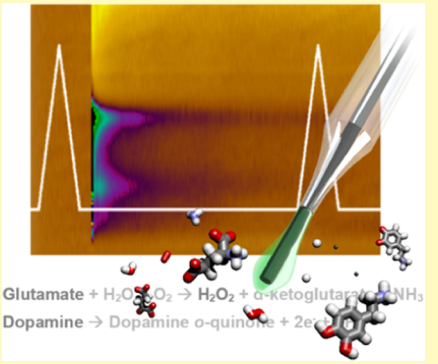

KEYWORDS: *FSCV, biosensor, carbon-fiber microelectrode, excitatory amino acid transporter, dl-threo-β-benzyloxyaspartic acid, dl-TBOA*

Measurement of neurochemical fluctuations and the interactions between different neurochemical species is vital to understanding the mechanisms underlying brain function and dysfunction. Glutamate and dopamine (DA) are two essential neurotransmitters in the striatum, a region of the brain involved in the initiation and coordination of movement and motor learning,[1,2] motivational salience,[3−5] and reward-seeking behavior.[6,7] However, improved methods for *in situ* detection are required to better establish the magnitude, time course, and relationship among these chemical signals. Real-time electroanalytical measurements of catecholamines have revealed the kinetics of DA release and reuptake in the striatum,[8−11] and how these are implicated in pathologies and specific motivated behaviors.[12−14] While electroanalytical techniques allow for straightforward, label-free quantification of catecholamines, relatively few neurotransmitters are electroactive, and as such, far more is known about catecholamine dynamics than other neurotransmitters, to date.

Glutamate is the most abundant excitatory neurotransmitter in the vertebrate brain and is a major component of at least 90% of excitatory synapses in humans.[15,16] Glutamate concentrations are highly regulated due to the potential for excitatory neurotoxicity.[17] Once released, glutamate is rapidly removed from the synapse via excitatory amino acid transporters (EAATs) present in both astrocytes and neurons.[18] Astrocyte reuptake is followed by conversion into glutamine, which is rereleased to neurons in a process that is thought to minimize glutamatergic excitotoxicity.[17,19] After reuptake by neurons, glutamine is converted back into glutamate, completing the cycle.[17,19−21] In addition to classical synaptic transmission, ongoing research also supports more complex glutamate release mechanisms, including synaptic spillover[22−25] and glutamate release by glial cells via exocytosis[26,27]

Received: June 23, 2023
Revised: October 24, 2023
Accepted: November 1, 2023
Published: November 14, 2023

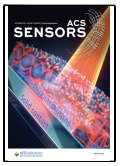

https://doi.org/10.1021/acssensors.3c01267
ACS Sens. 2023, 8, 4091−4100

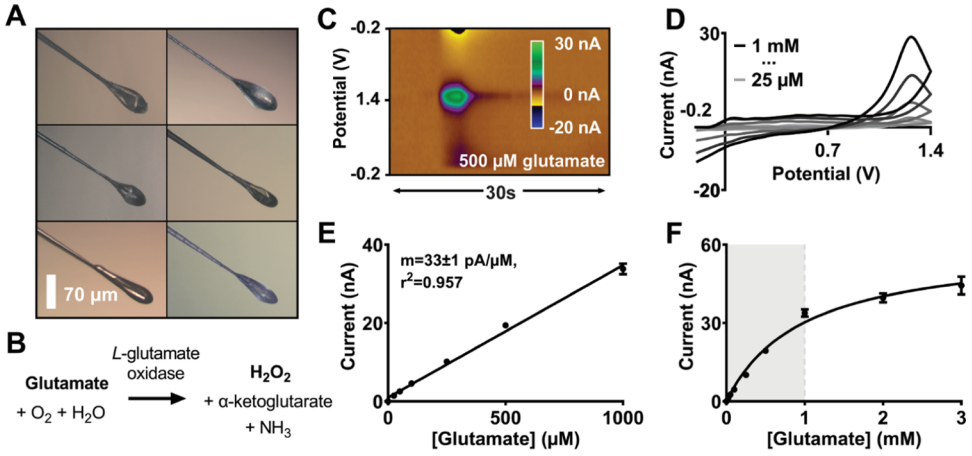

Figure 1. Characterization of the glutamate microbiosensor. (A) Magnified view of electrodeposited GlutOx-chitosan hydrogels. (B) Enzymatic generation of electroactive H_2O_2 by way of GlutOx. (C) Representative color plot constructed from background-subtracted voltammograms obtained in the detection of 500 μM glutamate, plotted with respect to potential (y-axis) and time (x-axis), with current plotted in false color. (D) Representative voltammograms for H_2O_2 that was enzymatically generated in response to increasing concentrations of glutamate. (E) Linear calibration curve ranging from 25 μM to 1 mM (n = 5). (F) A Michaelis–Menten-like response is observed over an extended concentration range (n = 5, r^2 = 0.905).

or a cysteine-glutamate exchanger.[26,28] Dysregulation of this transport system is suspected to disrupt glutamate homeostasis by shifting basal extracellular glutamate concentrations, which is believed to play a role in the maladaptive behaviors associated with drug abuse and relapse.[29−31]

The striatum receives substantial glutamatergic input from the premotor and prefrontal cortices.[32,33] Notably, a subpopulation of DA terminals in striatum can release both glutamate and DA from segregated release sites on a single neuron.[34] It has also been suggested that glutamate may serve as a modulator of the vesicular packaging of DA in striatum[35] and that glutamate and DA can reciprocally modulate the release and reuptake of the other.[36,37] While great progress has been made in understanding glutamate and DA signaling individually, many questions remain unanswered regarding how these signals work in combination to influence striatal function in various contexts. To address these questions, both neurotransmitters must be monitored in real time at single recording sites.

In this work, we present a novel microbiosensor for the detection of both glutamate and DA, created through the entrapment of glutamate oxidase (GlutOx) within a chitosan hydrogel matrix electrodeposited onto carbon-fiber microelectrodes. These sensors were created following existing strategies that utilize oxidase enzymes for the subsecond detection of glucose[38−41] and lactate[41,42] fluctuations *in vivo* using fast-scan cyclic voltammetry (FSCV). Such enzyme-modified carbon-fiber microelectrodes generate hydrogen peroxide (H_2O_2) in the presence of the enzyme substrate, which is then readily oxidized at the electrode surface.[43] Unlike other enzymes used for glutamate detection, GlutOx requires only O_2 and H_2O as cosubstrates, along with a covalently bound FAD cofactor.[44,45]

Notably, existing biosensors utilizing GlutOx have almost exclusively been coupled with fixed-potential, amperometric detection of glutamate by way of GlutOx-generated H_2O_2.[46,47] This approach renders simultaneous detection of other co-analytes impossible using a single biosensor. Due to the inherent nonselectivity of amperometric sensing, these probes are engineered with coatings and/or surface modifications designed to exclude all other electroactive species, which would otherwise be oxidized at the electrode surface at the overpotentials required to oxidize H_2O_2 (for review, see Wahono et al.[48]). In contrast, our glutamate microbiosensor is completely different; it is coupled with FSCV to enable not only measurement of the target analyte (glutamate) but also all other electroactive species present which generate distinct signature voltammograms. This innovative approach enables the simultaneous detection of multiple species whose contributions can be further disentangled with multivariate regression techniques, such as principal component regression (PCR).[49,50] Our voltammetric sensing strategy reframes "interferents" (within the context of amperometry) as co-analytes, and eliminates the need for exclusion layers that complicate fabrication and can be detrimental to performance, particularly with respect to sensor response time.[51] As such, our microbiosensor enables deliberate quantification of electroactive species released concurrently with glutamate, allowing for the first simultaneous measurements of DA and glutamate at single recording sites.

The voltammetric waveform employed in this work was optimized to leverage the suitability of the technique for the simultaneous detection of both glutamate and DA. The microbiosensors have been characterized for their sensitivity to and selectivity for both species. Biosensor stability has been assessed over extended recording periods and under varying O_2 concentrations. Finally, the microbiosensors were pharmacologically validated in rat brain slices using glutamine and DL-threo-β-benzyloxyaspartic acid (DL-TBOA) to increase glutamate production and inhibit glutamate reuptake, respectively.[52] Overall, these experiments characterize an important new research tool that moves the state of the art for glutamate quantification in the brain from the detection of one species at a time to the simultaneous real-time monitoring of multiple neurochemicals.

RESULTS

Characterization of the Glutamate Microbiosensor. Glutamate microbiosensors were fabricated as described in the Methods section, and visually inspected to verify uniformity

https://doi.org/10.1021/acssensors.3c01267
ACS Sens. 2023, 8, 4091−4100

Table 1. Comparison Of Glutamate Microbiosensor Performance

authors	technique	linear range	glutamate sensitivity	sensitivity normalized to electrode area (nA/μM/μm^2)
Wassum et al.[56]	amperometry	10−100 μM	2.4 pA/μM	5×10^{-7}
Wassum et al.[57]	amperometry	5−60 μM	7 pA/μM	1.5×10^{-6}
Soldatkina et al.[58]	amperometry	2.5−400 μM	0.5 nA/μM	3.9×10^{-6}
Oldenziel et al.[59]	amperometry	not given	8.5 pA/μM	max 8.9×10^{-7}
Batra et al.[60]	amperometry	5−500 μM	not given	1.6×10^{-6}
Frey et al.[61]	amperometry	max 5 μM	13.3 pA/μM	1.8×10^{-6}
Wang et al.[51]	amperometry	10−100 μM	not given	1.3×10^{-6}
Chen et al.[62]	amperometry	0 050−40 μM	24 nA/μM	3.1×10^{-3}
Pinnacle[63]	amperometry	max 50 μM	max 1.2 nA/μM	4.7×10^{-5}
this work	FSCV	25−1000 μM	33 pA/μM	1.5×10^{-5}

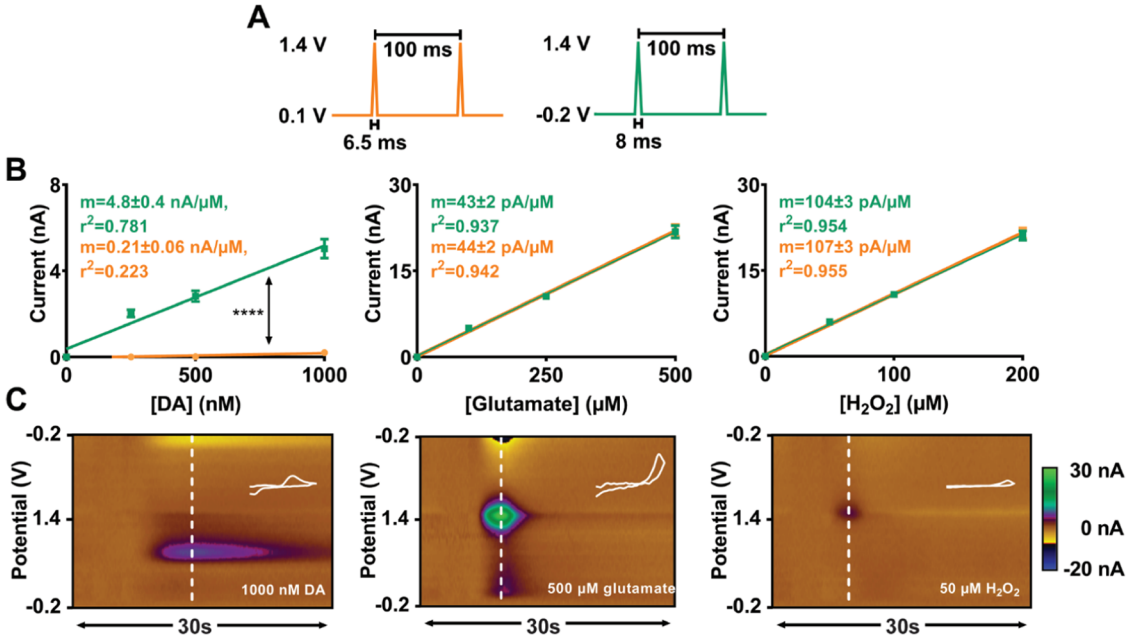

Figure 2. Sensitivity to DA, glutamate, and H_2O_2. (A) Triangular potential waveforms applied at 10 Hz and 400 V/s. Between scans, the potential is held at +0.1 V (orange) or −0.2 V (green). (B) Calibration curves obtained using these waveforms for detection of (left) DA (0−1000 nM, n = 4), (middle) glutamate (0−500 μM, n = 4), and (right) H_2O_2 (0−200 μM, n = 4). Sensitivity to DA is significantly improved using a −0.2 V holding potential (one-way ANCOVA, ****$p < 0.0001$). (C) Representative color plots of background-subtracted voltammograms corresponding to the analytes shown in (B). The current range shown in each color plot is identical across all three panels.

(Figure 1A). Here, the glass insulation is visible on the shaft of the electrode, but the carbon-fiber sensing surface is obscured by the chitosan hydrogel. The hydrogel measures about 30 μm in diameter, a size that offers precise spatial resolution and that results in minimal tissue damage. The microbiosensors were evaluated in a benchtop flow cell to characterize their performance (Figure 1C−F). Cyclic voltammograms and color plots generated in response to bolus applications of glutamate (25 μM to 3 mM) were consistent with voltammograms for H_2O_2,[53] indicating the successful conversion of glutamate to H_2O_2 by the entrapped GlutOx enzyme (Figure 1B−D). A linear current response was observed between 25 μM and approximately 1 mM glutamate, indicating a glutamate sensitivity of 33 ± 1 pA/μM (r^2 = 0.957, n = 5, Figure 1E). Over the full range of glutamate concentrations tested, a Michaelis−Menten-like response was observed in which the measured current approached a maximum value. This behavior is commonly observed in enzyme-based biosensors and occurs due to the finite amount of enzyme present on the sensor. When the enzyme becomes saturated with analyte, additional conversion is not possible, leading to a maximum level of response. The glutamate microbiosensors were characterized to establish the maximum current generated in response to glutamate (I_{max} = 60 ± 3 nA), as well as the glutamate concentration corresponding to a half-maximal current response (k_M = 1.0 ± 0.1 mM, r^2 = 0.905, n = 5, Figure 1F). Similar biosensors using GlutOx have reported k_M values in the range of 0.5−0.9 mM,[54,55] which aligns well with our results.

The glutamate biosensor described here is fabricated from carbon-fiber microelectrodes, which are well characterized for voltammetry and are very well suited for precise surgical targeting of specific brain structures. Table 1 directly compares performance with several previously described biosensor technologies, which have demonstrated sensitivities to glutamate in the picoampere-to-nanoampere per micromolar range,[56−59] and boast a linear response in the low-micromolar to several-hundred-micromolar range.[51,56−58,60,61] Notably, the microbiosensor described herein is smaller (nominally around 2200 μm^2 of electroactive surface area) than many of the conventional glutamate sensors, which have electroactive surface areas in the range of ∼5000 μm^2 to greater than 0.1

https://doi.org/10.1021/acssensors.3c01267
ACS Sens. 2023, 8, 4091−4100

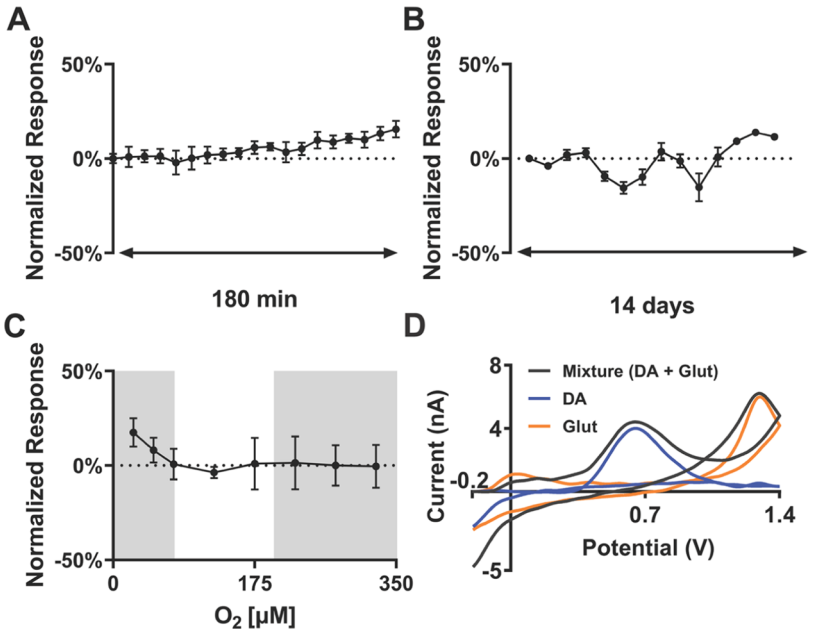

Figure 3. Microbiosensor stability. (A) Over 3 h of continuous use, no significant change was observed in the microbiosensor response to glutamate (500 μM, $p > 0.05$). Sensitivity to glutamate was also stable (B) over a 14-day sampling period ($p > 0.05$) and (C) under varying concentrations of dissolved O_2 ($p > 0.05$). O_2 concentrations that exceed the physiological range are indicated in gray. Repeated-measures one-way ANOVA, $n = 4$. (D) Direct comparison of representative CVs for a mixture containing both DA (1 μM) and glutamate (250 μM) to CVs collected for each analyte individually at the same concentrations on the same microbiosensor.

mm^2.[56−58,60−62] Despite the much smaller size, our sensor exhibits both a high sensitivity to glutamate and a high detection efficiency when the performance is normalized to the electrode surface area.

The complex transduction schemes that are generally employed at glutamate biosensors involve functionalization beyond the deposition of GlutOx (e.g., the inclusion of redox mediators, nanoparticles, chemically selective films, etc.). Inclusion of these components can boost sensitivity to glutamate, but necessitates additional fabrication procedures and can result in a comparatively limited linear response range.[62] Another important factor to consider is inherent in the relationship between the thickness of the functional coating and response time. Sensors optimized for speed omit selectivity membranes and minimize enzyme loading to a thin conformal layer to substantially reduce diffusional delay, resulting in submillisecond temporal resolution.[51] However, a reduction in enzyme loading also results in reduced sensitivity and enzyme saturation at noticeably lower glutamate concentrations, as indicated by the small k_M values. Finally, it is important to note that while amperometry enables rapid sensing, it does not provide much in terms of qualitative information. As such, fast amperometric sensors lacking selectivity membranes are more vulnerable to unwanted signal contributions from interferents.[51]

Waveform Optimization for the Co-Detection of Glutamate and DA. DA is electroactive and frequently investigated using electroanalytical techniques.[63,64] However, when targeting glutamate with an amperometric biosensor, it is an interferent of special concern because it is abundant in the striatum and oxidized at potentials below the oxidation potential of H_2O_2. Our novel voltammetric approach allows for DA to be investigated as a secondary analyte at the same sensor. Voltammetric waveforms for DA detection typically use a holding potential of −0.4 V. This leverages electrostatic attraction between the negatively charged electrode and positively charged DA to preconcentrate DA at the sensor surface, improving sensitivity.[38,41] By contrast, prior work has established that biosensor performance for the targeted nonelectroactive analyte is improved when less negative holding potentials are utilized.[38] Here, the GlutOx microbiosensor response to DA, glutamate, and H_2O_2 was evaluated in order to determine an optimal holding potential for co-detection of DA and glutamate. Two different waveforms were investigated using a scan rate of 400 V/s applied at a frequency of 10 Hz (Figure 2A, potential limits of +0.1 to +1.4 V (orange) and −0.2 to +1.4 V (green)). Sensitivity to DA improved from 0.21 ± 0.06 to 4.8 ± 0.4 nA/μM ($n = 4$, $r^2 =$ 0.223, 0.781) when the negative holding potential was incorporated, representing a more than 2000-fold improvement in DA sensitivity (one-way analysis of covariance (ANCOVA), ****$p < 0.0001$, Figure 2B).

Sensitivities to glutamate and to nonenzymatic H_2O_2 were also investigated with both waveforms. This is important because there are several sources of endogenous H_2O_2 in the brain. In the striatum, H_2O_2 serves as a modulator of DA signaling,[65−67] and in excess it is involved in pathological states.[68] Because the microbiosensor described in this work relies on the detection of H_2O_2 as a proxy for glutamate, the infiltration of endogenous (nonenzymatic) H_2O_2 into the chitosan hydrogel represents a possible source of interference, even when FSCV is used. However, supraphysiological concentrations of H_2O_2 (50 μM) generated substantially less current than physiological concentrations of glutamate (Figure 2B,C), which have been estimated to be in the range of 160 μM (in the extrasynaptic space) to greater than 1 mM (within the synaptic cleft) during normal vesicular release,[69] and potentially even greater in pathological states.[70] Consistent with prior reports, sensitivity to nonenzymatic H_2O_2 was attenuated at the biosensors as compared to control carbon

https://doi.org/10.1021/acssensors.3c01267
ACS Sens. 2023, 8, 4091−4100

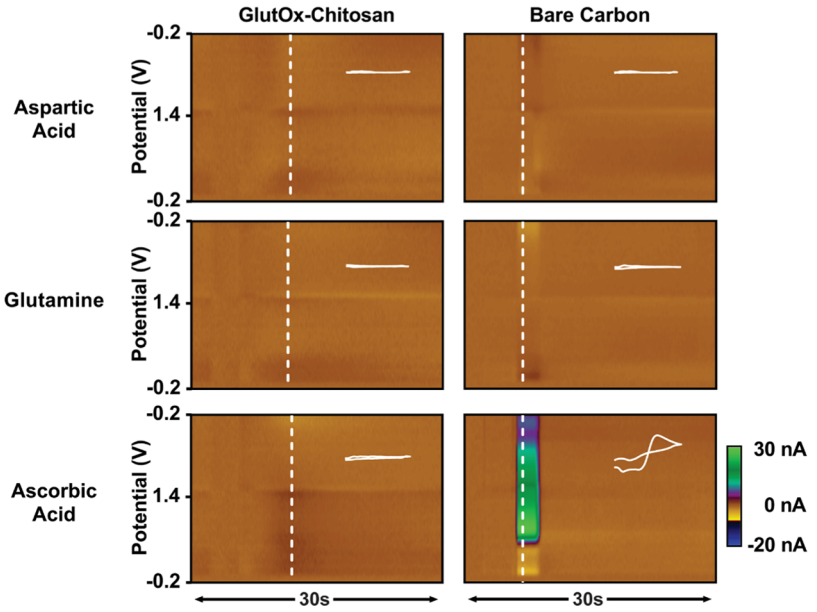

Figure 4. Representative color plots showing the current response to bolus injections of potential interferents: aspartic acid (10 μM), glutamine (10 μM), and ascorbic acid (100 μM). Although ascorbic acid was detected using the classic bare carbon-fiber microelectrode, none of these species was detected at the microbiosensor. Insets: cyclic voltammograms extracted from the data at the time indicated by the dotted vertical line. The current range shown in each color plot is identical across all six panels.

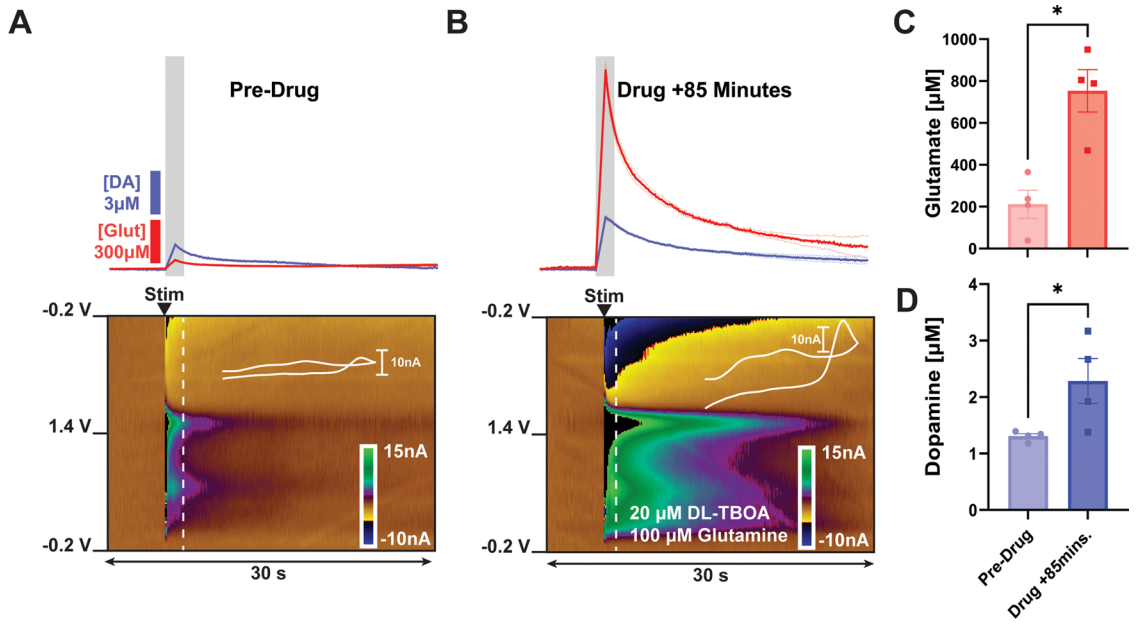

Figure 5. Simultaneous, real-time detection of glutamate (red) and DA (blue) at a single recording site in the striatum. (A,B) Top: Representative concentration versus time traces for both analytes collected in response to local stimulation, showing concentrations averaged over three replicate files. Bottom: Color plots of the raw voltammetric data corresponding to the traces above and showing characteristic redox peaks for DA and glutamate. Cyclic voltammograms extracted from these raw data are inset in white. Data were collected (A) before and (B) after bath application of 20 μM dl-TBOA, an EAAT inhibitor, and 100 μM glutamine, a glutamate precursor. Bottom:Top: olor plots After drug exposure, the evoked glutamate signal was both larger and slower to decay. (C) Across the entire data set (n = 4 animals), evoked glutamate concentrations were significantly elevated after 85 min of drug exposure (*p < 0.05). (D) Evoked DA concentrations also increased (*p < 0.05, one-tailed paired t test, n = 4).

microelectrodes lacking the hydrogel coating (data not shown).[38] At the hydrogel-coated biosensors, sensitivity to glutamate was indistinguishable across the tested waveforms (one-way ANCOVA, p > 0.05), indicating that a −0.2 V holding potential improves sensitivity to DA without compromising glutamate detection. These results are consistent with prior work in our lab using similar microbiosensors for the simultaneous detection of glucose and DA.[38] Thus, all subsequent characterization described herein utilized the −0.2 to +1.4 V triangular waveform (Figure 2A, green).

***In Vitro* Characterization of Stability and Selectivity.** Glutamate microbiosensors were characterized for stability during use and over a 2-week storage period (Figure 3). Across 3 h of continuous use, a single concentration of glutamate was

https://doi.org/10.1021/acssensors.3c01267
ACS Sens. 2023, 8, 4091−4100

assessed in triplicate every 10 min. A small improvement in sensitivity was evident over this time, as is common with continuous cycling of carbon-based sensors,[71] but a repeated-measures one-way analysis of variance (ANOVA) demonstrates that no significant change in the signal occurred during this time period ($p > 0.05$, $n = 4$, Figure 3A). Next, electrodes were stored in refrigerated phosphate-buffered saline (PBS) and evaluated by daily triplet injections of glutamate (500 μM) over a 2-week period. The data demonstrate no significant change in sensitivity to glutamate between the first and final days of measurement (one-way ANOVA, $p > 0.05$, $n = 4$, Figure 3B). Next, the microbiosensor response to injections of a single concentration of glutamate was evaluated at varying concentrations of dissolved O_2, due to the dependency of GlutOx on O_2 as a cosubstrate. In the brain, physiological O_2 concentrations vary over a fairly limited range, even with a large external stimulation.[72] The current generated in response to glutamate did not significantly change across a wide range of O_2 concentrations (25−325 μM, one-way ANOVA, $p > 0.05$, $n = 4$, Figure 3C). Finally, it has been reported that glutamate can electropolymerize on a bare carbon electrode surface, affecting sensitivity to DA.[73] This was not evident in the data collected using our hydrogel-coated carbon electrodes. Figure 3D directly compares the voltammetric response for a mixture of both DA (1 μM) and glutamate (250 μM) to voltammograms for each analyte recorded individually at the same concentrations and on the same sensor. The presence of glutamate did not affect the sensitivity to DA, and vice versa.

Another set of experiments was aimed at evaluating selectivity by assessing microbiosensor performance in response to potential interferents such as ascorbic acid (100 μM, $n = 7$), aspartate (10 μM, $n = 5$), and glutamine (10 μM, $n = 5$). Of note, ascorbic acid is electroactive, but it exhibits a unique voltammetric signature allowing it to be readily distinguished from DA at a bare electrode.[74,75] Aspartate was investigated because GlutOx can exhibit a miniscule response to aspartate (<1% that of glutamate at physiological pH).[44] Glutamine is structurally similar to glutamate, and it is abundant in the brain as an integral component of glutamate metabolism.[76,77] A negligible amount of current was generated at the microbiosensor in response to all of these species (Figure 4).

Detection of Glutamate Release in Brain Slices. To validate the performance in live tissue, the glutamate microbiosensors were placed in acute rat brain slices to measure the electrically evoked release of glutamate and DA at discrete locations in the ventral striatum (Figure 5A,B). The results demonstrate the simultaneous detection of (electroactive) DA and (nonelectroactive) glutamate in response to a biphasic electrical stimulus ($n = 4$ animals). To validate the glutamate signal, slices were perfused with a solution of glutamine (100 μM), a metabolic precursor to glutamate,[76,77] and DL-TBOA (20 μM), a potent inhibitor of the EAATs responsible for glutamate reuptake.[52] Over the course of ∼85 min, the evoked glutamate signal significantly increased in magnitude, more than doubling between the time of drug application and the end of the experiment (one-tailed paired t test, $^*p < 0.05$, Figure 5C). The amplitude of the DA signal also exhibited a modest increase (one-tailed paired t test, $^*p < 0.05$, Figure 5D). While DL-TBOA treatment has no known specific effect on DA reuptake,[31] the supraphysiological release of glutamate observed in this experiment may have served to potentiate DA release, as observed in other works.[78] In fact, prior studies have suggested a facilitatory relationship between glutamate and DA release,[79] possibly involving synergistic vesicular loading.[35] Supraphysiological glutamate agonism has also been shown to elicit substantial increases in extracellular DA,[80,81] in a manner that may be unrelated to normal, physiological interactions between these neurotransmitters.[82]

CONCLUSIONS

Substantial research into the striatum has revealed the importance of interplay among multiple neurotransmitters to the functioning of this brain region and the various pathologies that can result from dysfunction. Continued research into the neurobiology of the striatum will necessitate the simultaneous quantification of distinct neurochemical species, including glutamate and DA. Our novel glutamate microbiosensor advances the state of the art by providing a powerful tool for the direct investigation of glutamate and DA at a single location with subsecond temporal resolution. This technological advance is transformative because it unlocks new opportunities to probe the interactions between these two species and to investigate their role in behavior in a way that has previously not been possible. It promises to uncover how the coordination of these molecules relates to the integration of motor impulses into coordinated movements and the transition from normal motivational salience to maladaptive drug-seeking behavior.

METHODS

Chemicals. All chemicals were used as received and purchased from Sigma-Aldrich, unless otherwise noted. Slice experiments were performed in artificial cerebrospinal fluid (aCSF; 119 mM NaCl, 2.5 mM KCl, 1 mM $NaH_2PO_4{\cdot}H_2O$, 26.2 mM $NaHCO_3$, 11 mM D(+)-glucose, 1.3 mM $MgSO_4{\cdot}7H_2O$, 2.5 mM CaCl), made as a 10× stock solution, and diluted to 1× on the day of the experiment. Compressed O_2, argon, and 5% CO_2/95% O_2 mixtures were purchased from ARC3 Gases.

Carbon-Fiber Microelectrode Fabrication. Carbon-fiber microelectrodes were fabricated as described in earlier work.[53,63] To summarize, an individual carbon fiber (7 μm diameter, T-650, Cytec Industries) was aspirated into a borosilicate glass capillary (10 cm long, 0.5 mm I.D., A-M systems) using a vacuum pump. A vertical micropipet puller (PE-21, Narishige) was used to heat the central region of each capillary and to pull it into two tapered sections. Each microelectrode was then trimmed under a microscope by using a scalpel such that approximately 100 μm of fiber was exposed beyond the carbon-glass interface. Electrodes were addressed by soldering a gold pin (Newark Element 14, Palatine, IL) to the end of a partially insulated wire (30 ga, Squires Electronics), coating the exposed end of the wire with conductive silver paint (Silver Print II, GC Electronics), and threading the coated wire into the open end of the capillary. The capillary and wire were then sealed together using a short section of heat shrink tubing.

Enzyme-Modified Electrode Fabrication. A 2% chitosan solution was prepared in 87 mM acetic acid and allowed to stand at room temperature until a pH of approximately 5.2 was reached. L-Glutamate oxidase (5 units from *Streptomyces* sp., Sigma-Aldrich) was dissolved in 57 μL of DI water. This solution was gently mixed with 150 μL of the 2% chitosan solution until homogenized and then stored at 4 °C for 24 h. To create glutamate microbiosensors, microelectrodes were first preconditioned in PBS (+0.1 to +1.4 V, 400 V/s) for 20 min at 60 Hz followed by 10 min at 10 Hz. Immediately after preconditioning, microelectrodes were lowered into the enzyme-bearing deposition solution in a custom deposition cell fabricated in-house. Electrodeposition was performed with a voltammetric sweep from a starting potential of 0 V to a final potential of −3.25 V at 25 mV/s. Enzyme-modified electrodes were immediately inspected and

https://doi.org/10.1021/acssensors.3c01267
ACS Sens. 2023, 8, 4091−4100

stored in PBS at 4 °C for a minimum of 12 h prior to use. On experiment day, biosensors were conditioned using a triangular waveform (+0.1 to +1.4 V, 400 V/s applied at 60 Hz for 20 min, followed by −0.2 to +1.4 V, 400 V/s, 10 Hz) until a stable background current was observed.

Microbiosensor Characterization. All *in vitro* characterization experiments were performed in a grounded Faraday cage using a custom-made flow-cell apparatus in which electrodes were suspended in the center of a continuous stream of buffer solution by a micromanipulator (KITE-R, World Precision Instruments). PBS was delivered to the flow cell inlet using a syringe pump (1 mL/min, NE-300, New Era Pump Systems). Analyte was reproducibly introduced to the buffer stream using a 6-port HPLC valve controlled by a pneumatic actuator (A60, Valco Instruments). For stability experiments spanning multiple days, electrodes were stored at 4 °C in PBS when not in use. For O_2 dependence experiments, concentrations of dissolved O_2 were manipulated by bubbling the sample with compressed O_2 or argon gas and measuring the dissolved O_2 concentration using a commercial O_2 sensor (Orion Star A213, Fisher Scientific) immediately prior to analyte injection.

Electrochemical Measurements. Electrochemical measurements were made using a potentiostat (Universal Electrochemistry Instrument (UEI), University of North Carolina Department of Chemistry Electronics Facility) interfaced with a head-stage amplifier (Pine Research Instruments). Potentiostat control and data acquisition were accomplished using HDCV software (University of North Carolina Department of Chemistry Electronics Facility) interfaced with the potentiostat through a PCI Express multifunction I/O device (PCIe-6363, National Instruments). Unless otherwise noted, all electrochemical measurements were made using a triangular waveform (−0.2 to +1.4 V vs Ag|AgCl, 400 V/s, −0.2 V holding potential, 10 Hz) over a 30 s recording window, using a 2 kHz, two-pole Sallen-Key analogue low-pass filter. Background subtraction and digital filtering were performed after data acquisition using HDCV Analysis software (University of North Carolina Department of Chemistry Electronics Facility). To better interpret current changes over time and across potential sweeps, color plots were assembled by concatenating sequentially collected cyclic voltammograms obtained over the full recording window with sampled currents depicted in color.

Animal Subjects and Care. All animal care and use procedures followed North Carolina State University Institutional Animal Care and Use Committee (IACUC) guidelines and the NIH's Guide for the Care and Use of Laboratory Animals. Male Sprague−Dawley rats (275−300 g, Charles River Laboratories) were pair housed in a temperature- and humidity-controlled environment (12 h/12 h light−dark cycle, ad libitum access to food and water) for at least 2 days prior to experiment.

Brain Slice Experiments. Rats were deeply anesthetized with 5% isoflurane gas and immediately decapitated. Brains were rapidly extracted and sectioned into 400 μm thick slices using a vibratome (NVSL, World Precision Instruments). Striatal slices were transferred to a holding chamber containing room-temperature aCSF bubbled with a CO_2/O_2 mixture (5% CO_2, balance O_2) and allowed to rest for 1 h. For measurements, brain slices were immobilized in a perfusion chamber mounted in the path of an upright microscope (Eclipse FN1, Nikon) enclosed in a grounded Faraday cage. Slices were perfused with aCSF bubbled with the CO_2/O_2 mixture using a peristaltic pump (1 mL/min, Minipuls 3, Gilson). Microbiosensors were inserted into the nucleus accumbens (NAc) core using a micromanipulator (LBM-7, Scientifica). A tungsten stimulating electrode (UEWMGESE0N2M, FHC Inc.) was interfaced with a biphasic current stimulator (DS4, Digitimer). Voltammetric recordings were collected every 5 min in response to biphasic stimulation (250 μA, 20 Hz, and 5−20 pulses). Three replicate recordings were obtained for each time point (±5 min).

Data Analysis and Statistics. Individual analytes were resolved from complex voltammetric data using PCR, performed with HDCV Analysis. Training sets were constructed of cyclic voltammograms collected *in vitro* for standards of glutamate, DA, and small shifts in pH that span the physiological range. Calibration factors for each analyte were determined by using linear regression. Training sets were evaluated for quality by confirming the orthogonality of the identified components and by visual inspection of the reproduced voltammograms for each analyte. Data were selected for quantification based on the 95% confidence threshold (Q_a). Variation observed in the traces immediately after the electrical stimulation (stimulation artifacts) was omitted from analysis. All stated and plotted values are given as the mean ± the standard error of the mean (SEM). Limit of detection was defined as 3 times the standard deviation of the noise. Prism 9 (GraphPad) was used for data analysis. Repeated-measures, one-way ANOVA and one-way ANCOVA with Tukey's multiple comparisons tests were used to establish significance. For brain slice experiments, a one-tailed paired *t* test was used to compare the data before and after pharmacological treatment. In all cases, the significance was determined with a 95% confidence limit.

AUTHOR INFORMATION

Corresponding Author

Leslie A. Sombers − *Department of Chemistry and Comparative Medicine Institute, North Carolina State University, Raleigh, North Carolina 27695, United States;* orcid.org/0000-0002-0978-9795; Email: Leslie_Sombers@ncsu.edu

Authors

Laney C. Kimble − *Department of Chemistry, Department of Biological Sciences, and Comparative Medicine Institute, North Carolina State University, Raleigh, North Carolina 27695, United States;* orcid.org/0000-0001-7505-9259

Jack S. Twiddy − *Department of Chemistry and Comparative Medicine Institute, North Carolina State University, Raleigh, North Carolina 27695, United States; Joint Department of Biomedical Engineering, North Carolina State University and University of North Carolina at Chapel Hill, Raleigh, North Carolina 27695, United States;* orcid.org/0000-0003-1929-5796

Jenna M. Berger − *Department of Chemistry, North Carolina State University, Raleigh, North Carolina 27695, United States*

Alexandra G. Forderhase − *Department of Chemistry, North Carolina State University, Raleigh, North Carolina 27695, United States*

Gregory S. McCarty − *Department of Chemistry, North Carolina State University, Raleigh, North Carolina 27695, United States*

John Meitzen − *Department of Biological Sciences and Comparative Medicine Institute, North Carolina State University, Raleigh, North Carolina 27695, United States*

Complete contact information is available at: https://pubs.acs.org/10.1021/acssensors.3c01267

Author Contributions

⊥L.C.K. and J.S.T. contributed equally. L.C.K. and J.S.T. contributed to experimental design, data collection, data analysis, data interpretation, and manuscript preparation. J.M.B., A.G.F., and G.S.M. contributed to experimental design, data analysis, and data interpretation. J.M. contributed to experimental design, data interpretation, and manuscript preparation. L.A.S. contributed to experimental design, data analysis, data interpretation, and manuscript preparation.

https://doi.org/10.1021/acssensors.3c01267
ACS Sens. 2023, 8, 4091−4100

Funding

This work was funded through a grant from the National Institute of Health to commercialize these probes with Pinnacle Technologies, Inc. (NIH R44MH119870).

Notes

The authors declare no competing financial interest.
Safety Statement: The authors do not have any unexpected or significant hazards or risks to report for this study.

■ ACKNOWLEDGMENTS

The authors acknowledge Jovica Todorov for experimental assistance and Pinnacle Technologies, Inc., for helpful discussion. L.C.K. acknowledges a Beckman Scholars Award from the Arnold and Mabel Beckman Foundation.

■ REFERENCES

(1) Graybiel, A. M.; Aosaki, T.; Flaherty, A. W.; Kimura, M. The Basal Ganglia and Adaptive Motor Control. *Science* **1994**, *265* (5180), 1826−1831.
(2) Hikosaka, O. Neural Systems for Control of Voluntary Action–a Hypothesis. *Adv. Biophys.* **1998**, *35*, 81−102.
(3) Zink, C. F.; Pagnoni, G.; Chappelow, J.; Martin-Skurski, M.; Berns, G. S. Human Striatal Activation Reflects Degree of Stimulus Saliency. *NeuroImage* **2006**, *29* (3), 977−983.
(4) Puglisi-Allegra, S.; Ventura, R. Prefrontal/Accumbal Catecholamine System Processes High Motivational Salience. *Front. Behav. Neurosci.* **2012**, *6*, 31.
(5) Berridge, K. C. From Prediction Error to Incentive Salience: Mesolimbic Computation of Reward Motivation. *Eur. J. Neurosci.* **2012**, *35* (7), 1124−1143.
(6) White, F. J.; Kalivas, P. W. Neuroadaptations Involved in Amphetamine and Cocaine Addiction. *Drug Alcohol Depend.* **1998**, *51* (1−2), 141−153.
(7) Balleine, B. W.; Delgado, M. R.; Hikosaka, O. The Role of the Dorsal Striatum in Reward and Decision-Making. *J. Neurosci.* **2007**, *27* (31), 8161−8165.
(8) Kuhr, W. G.; Ewing, A. G.; Caudill, W. L.; Wightman, R. M. Monitoring the Stimulated Release of Dopamine with in Vivo Voltammetry. I: Characterization of the Response Observed in the Caudate Nucleus of the Rat. *J. Neurochem.* **1984**, *43* (2), 560−569.
(9) Stamford, J. A.; Kruk, Z. L.; Millar, J.; Wightman, R. M. Striatal Dopamine Uptake in the Rat: In Vivo Analysis by Fast Cyclic Voltammetry. *Neurosci. Lett.* **1984**, *51* (1), 133−138.
(10) Jones, S. R.; Garris, P. A.; Kilts, C. D.; Wightman, R. M. Comparison of Dopamine Uptake in the Basolateral Amygdaloid Nucleus, Caudate-Putamen, and Nucleus Accumbens of the Rat. *J. Neurochem.* **1995**, *64* (6), 2581−2589.
(11) Calipari, E. S.; Huggins, K. N.; Mathews, T. A.; Jones, S. R. Conserved Dorsal-Ventral Gradient of Dopamine Release and Uptake Rate in Mice, Rats and Rhesus Macaques. *Neurochem. Int.* **2012**, *61* (7), 986−991.
(12) Addy, N. A.; Daberkow, D. P.; Ford, J. N.; Garris, P. A.; Wightman, R. M. Sensitization of Rapid Dopamine Signaling in the Nucleus Accumbens Core and Shell after Repeated Cocaine in Rats. *J. Neurophysiol.* **2010**, *104* (2), 922−931.
(13) Aragona, B. J.; Cleaveland, N. A.; Stuber, G. D.; Day, J. J.; Carelli, R. M.; Wightman, R. M. Preferential Enhancement of Dopamine Transmission within the Nucleus Accumbens Shell by Cocaine Is Attributable to a Direct Increase in Phasic Dopamine Release Events. *J. Neurosci.* **2008**, *28* (35), 8821−8831.
(14) Cameron, C. M.; Wightman, R. M.; Carelli, R. M. Dynamics of Rapid Dopamine Release in the Nucleus Accumbens during Goal-Directed Behaviors for Cocaine versus Natural Rewards. *Neuropharmacology* **2014**, *86*, 319−328.
(15) Samardzic, J.; Jadzic, D.; Hencic, B.; Jancic, J.; Strac, D. S. Introductory Chapter: GABA/Glutamate Balance: A Key for Normal Brain Functioning. In *GABA and Glutamate − New Developments in Neurotransmission Research*; Samardzic, J., Ed.; InTech, 2018.
(16) Meldrum, B. S. Glutamate as a Neurotransmitter in the Brain: Review of Physiology and Pathology. *J. Nutr.* **2000**, *130* (4), 1007S−1015S.
(17) Andersen, J. V.; Markussen, K. H.; Jakobsen, E.; Schousboe, A.; Waagepetersen, H. S.; Rosenberg, P. A.; Aldana, B. I. Glutamate Metabolism and Recycling at the Excitatory Synapse in Health and Neurodegeneration. *Neuropharmacology* **2021**, *196*, No. 108719.
(18) Malik, A. R.; Willnow, T. E. Excitatory Amino Acid Transporters in Physiology and Disorders of the Central Nervous System. *Int. J. Mol. Sci.* **2019**, *20* (22), 5671.
(19) Albrecht, J.; Sidoryk-Węgrzynowicz, M.; Zielińska, M.; Aschner, M. Roles of Glutamine in Neurotransmission. *Neuron Glia Biol.* **2010**, *6* (4), 263−276.
(20) Nicklas, W. J.; Zeevalk, G.; Hyndman, A. Interactions between Neurons and Glia in Glutamate/Glutamine Compartmentation. *Biochem. Soc. Trans.* **1987**, *15* (2), 208−210.
(21) Meriney, S. D.; Fanselow, E. E. Amino Acid Neurotransmitters. In *Synaptic Transmission*; Elsevier, 2019; pp 399−419.
(22) Zhang, H.; Sulzer, D. Glutamate Spillover in the Striatum Depresses Dopaminergic Transmission by Activating Group I Metabotropic Glutamate Receptors. *J. Neurosci.* **2003**, *23* (33), 10585−10592.
(23) Isaacson, J. S. Synaptic Transmission: Spillover in the Spotlight. *Curr. Biol.* **2000**, *10* (13), R475−R477.
(24) Hires, S. A.; Zhu, Y.; Tsien, R. Y. Optical Measurement of Synaptic Glutamate Spillover and Reuptake by Linker Optimized Glutamate-Sensitive Fluorescent Reporters. *Proc. Natl. Acad. Sci. U.S.A.* **2008**, *105* (11), 4411−4416.
(25) Syková, E. Extrasynaptic Volume Transmission and Diffusion Parameters of the Extracellular Space. *Neuroscience* **2004**, *129* (4), 861−876.
(26) Malarkey, E. B.; Parpura, V. Mechanisms of Glutamate Release from Astrocytes. *Neurochem. Int.* **2008**, *52* (1−2), 142−154.
(27) Harada, K.; Kamiya, T.; Tsuboi, T. Gliotransmitter Release from Astrocytes: Functional, Developmental, and Pathological Implications in the Brain. *Front. Neurosci.* **2016**, *9*, No. 499, DOI: 10.3389/fnins.2015.00499.
(28) Bridges, R. J.; Natale, N. R.; Patel, S. A. System Xc^- Cystine/Glutamate Antiporter: An Update on Molecular Pharmacology and Roles within the CNS. *Br. J. Pharmacol.* **2012**, *165* (1), 20−34.
(29) Reissner, K. J.; Kalivas, P. W. Using Glutamate Homeostasis as a Target for Treating Addictive Disorders. *Behav. Pharmacol.* **2010**, *21* (5−6), 514−522.
(30) Knackstedt, L. A.; Moussawi, K.; Lalumiere, R.; Schwendt, M.; Klugmann, M.; Kalivas, P. W. Extinction Training after Cocaine Self-Administration Induces Glutamatergic Plasticity to Inhibit Cocaine Seeking. *J. Neurosci.* **2010**, *30* (23), 7984−7992.
(31) Yang, H.-J.; Hempel, B. J.; Bi, G.-H.; He, Y.; Zhang, H.-Y.; Gardner, E. L.; Xi, Z.-X. Elevation of Extracellular Glutamate by Blockade of Astrocyte Glutamate Transporters Inhibits Cocaine Reinforcement in Rats via a NMDA-GluN2B Receptor Mechanism. *J. Neurosci.* **2022**, *42* (11), 2327−2343.
(32) Haber, S. N. Corticostriatal Circuitry. *Dialogues Clin. Neurosci.* **2016**, *18* (1), 7−21.
(33) Parent, A.; Cicchetti, F. The Current Model of Basal Ganglia Organization under Scrutiny. *Mov. Disord.* **1998**, *13* (2), 199−202.
(34) Zhang, S.; Qi, J.; Li, X.; Wang, H.-L.; Britt, J. P.; Hoffman, A. F.; Bonci, A.; Lupica, C. R.; Morales, M. Dopaminergic and Glutamatergic Microdomains in a Subset of Rodent Mesoaccumbens Axons. *Nat. Neurosci.* **2015**, *18* (3), 386−392.
(35) Hnasko, T. S.; Chuhma, N.; Zhang, H.; Goh, G. Y.; Sulzer, D.; Palmiter, R. D.; Rayport, S.; Edwards, R. H. Vesicular Glutamate Transport Promotes Dopamine Storage and Glutamate Corelease in Vivo. *Neuron* **2010**, *65* (5), 643−656.
(36) Morari, M.; Marti, M.; Sbrenna, S.; Fuxe, K.; Bianchi, C.; Beani, L. Reciprocal Dopamine-Glutamate Modulation of Release in the Basal Ganglia. *Neurochem. Int.* **1998**, *33* (5), 383−397.

(37) David, H. N.; Ansseau, M.; Abraini, J. H. Dopamine-Glutamate Reciprocal Modulation of Release and Motor Responses in the Rat Caudate-Putamen and Nucleus Accumbens of "Intact" Animals. *Brain Res. Rev.* **2005**, *50* (2), 336−360.
(38) Smith, S. K.; Lee, C. A.; Dausch, M. E.; Horman, B. M.; Patisaul, H. B.; McCarty, G. S.; Sombers, L. A. Simultaneous Voltammetric Measurements of Glucose and Dopamine Demonstrate the Coupling of Glucose Availability with Increased Metabolic Demand in the Rat Striatum. *ACS Chem. Neurosci.* **2017**, *8* (2), 272−280.
(39) Smith, S. K.; Lugo-Morales, L. Z.; Tang, C.; Gosrani, S. P.; Lee, C. A.; Roberts, J. G.; Morton, S. W.; McCarty, G. S.; Khan, S. A.; Sombers, L. A. Quantitative Comparison of Enzyme Immobilization Strategies for Glucose Biosensing in Real-Time Using Fast-Scan Cyclic Voltammetry Coupled with Carbon-Fiber Microelectrodes. *ChemPhysChem* **2018**, *19* (10), 1197−1204.
(40) Lugo-Morales, L. Z.; Loziuk, P. L.; Corder, A. K.; Toups, J. V.; Roberts, J. G.; McCaffrey, K. A.; Sombers, L. A. Enzyme-Modified Carbon-Fiber Microelectrode for the Quantification of Dynamic Fluctuations of Nonelectroactive Analytes Using Fast-Scan Cyclic Voltammetry. *Anal. Chem.* **2013**, *85* (18), 8780−8786.
(41) Forderhase, A. G.; Styers, H. C.; Lee, C. A.; Sombers, L. A. Simultaneous Voltammetric Detection of Glucose and Lactate Fluctuations in Rat Striatum Evoked by Electrical Stimulation of the Midbrain. *Anal. Bioanal. Chem.* **2020**, *412* (24), 6611−6624.
(42) Smith, S. K.; Gosrani, S. P.; Lee, C. A.; McCarty, G. S.; Sombers, L. A. Carbon-Fiber Microbiosensor for Monitoring Rapid Lactate Fluctuations in Brain Tissue Using Fast-Scan Cyclic Voltammetry. *Anal. Chem.* **2018**, *90* (21), 12994−12999.
(43) Wilson, G. S.; Johnson, M. A. In-Vivo Electrochemistry: What Can We Learn about Living Systems? *Chem. Rev.* **2008**, *108* (7), 2462−2481.
(44) Kusakabe, H.; Midorikawa, Y.; Kuninaka, A.; Yoshino, H. Occurrence of a New Enzyme, L-Glutamate Oxidase in a Wheat Bran Culture Extract of *Streptomyces* Sp. X-119−6. *Agric. Biol. Chem.* **1983**, *47* (1), 175−177.
(45) Arima, J.; Sasaki, C.; Sakaguchi, C.; Mizuno, H.; Tamura, T.; Kashima, A.; Kusakabe, H.; Sugio, S.; Inagaki, K. Structural Characterization of L-Glutamate Oxidase from *Streptomyces* Sp. X-119−6. *FEBS J.* **2009**, *276* (14), 3894−3903.
(46) Okon, S. L.; Ronkainen, N. J. Enzyme-Based Electrochemical Glutamate Biosensors. In *Electrochemical Sensors Technology*; Rahman, M. M.; Asiri, A. M., Eds.; InTech, 2017.
(47) Shin, M.; Wang, Y.; Borgus, J. R.; Venton, B. J. Electrochemistry at the Synapse. *Annu. Rev. Anal. Chem.* **2019**, *12* (1), 297−321.
(48) Wahono, N.; Qin, S.; Oomen, P.; Cremers, T. I. F.; de Vries, M. G.; Westerink, B. H. C. Evaluation of Permselective Membranes for Optimization of Intracerebral Amperometric Glutamate Biosensors. *Biosens. Bioelectron.* **2012**, *33* (1), 260−266.
(49) Keithley, R. B.; Wightman, R. M. Assessing Principal Component Regression Prediction of Neurochemicals Detected with Fast-Scan Cyclic Voltammetry. *ACS Chem. Neurosci.* **2011**, *2* (9), 514−525.
(50) Rodeberg, N. T.; Johnson, J. A.; Cameron, C. M.; Saddoris, M. P.; Carelli, R. M.; Wightman, R. M. Construction of Training Sets for Valid Calibration of in Vivo Cyclic Voltammetric Data by Principal Component Analysis. *Anal. Chem.* **2015**, *87* (22), 11484−11491.
(51) Wang, Y.; Mishra, D.; Bergman, J.; Keighron, J. D.; Skibicka, K. P.; Cans, A.-S. Ultrafast Glutamate Biosensor Recordings in Brain Slices Reveal Complex Single Exocytosis Transients. *ACS Chem. Neurosci.* **2019**, *10* (3), 1744−1752.
(52) Shimamoto, K.; Lebrun, B.; Yasuda-Kamatani, Y.; Sakaitani, M.; Shigeri, Y.; Yumoto, N.; Nakajima, T. Dl- *Threo* -*β*-Benzyloxyaspartate, A Potent Blocker of Excitatory Amino Acid Transporters. *Mol. Pharmacol.* **1998**, *53* (2), 195−201.
(53) Sanford, A. L.; Morton, S. W.; Whitehouse, K. L.; Oara, H. M.; Lugo-Morales, L. Z.; Roberts, J. G.; Sombers, L. A. Voltammetric Detection of Hydrogen Peroxide at Carbon Fiber Microelectrodes. *Anal. Chem.* **2010**, *82* (12), 5205−5210.
(54) Ford, R.; Quinn, S. J.; O'Neill, R. D. Characterization of Biosensors Based on Recombinant Glutamate Oxidase: Comparison of Crosslinking Agents in Terms of Enzyme Loading and Efficiency Parameters. *Sensors* **2016**, *16* (10), 1565.
(55) Govindarajan, S.; McNeil, C. J.; Lowry, J. P.; McMahon, C. P.; O'Neill, R. D. Highly Selective and Stable Microdisc Biosensors for L-Glutamate Monitoring. *Sens. Actuators, B* **2013**, *178*, 606−614.
(56) Wassum, K. M.; Tolosa, V. M.; Wang, J.; Walker, E.; Monbouquette, H. G.; Maidment, N. T. Silicon Wafer-Based Platinum Microelectrode Array Biosensor for Near Real-Time Measurement of Glutamate in Vivo. *Sensors* **2008**, *8* (8), 5023−5036.
(57) Wassum, K. M.; Tolosa, V. M.; Tseng, T. C.; Balleine, B. W.; Monbouquette, H. G.; Maidment, N. T. Transient Extracellular Glutamate Events in the Basolateral Amygdala Track Reward-Seeking Actions. *J. Neurosci.* **2012**, *32* (8), 2734−2746.
(58) Soldatkina, O. V.; Soldatkin, O. O.; Kasap, B. O.; Kucherenko, D. Y.; Kucherenko, I. S.; Kurc, B. A.; Dzyadevych, S. V. A Novel Amperometric Glutamate Biosensor Based on Glutamate Oxidase Adsorbed on Silicalite. *Nanoscale Res. Lett.* **2017**, *12* (1), 260.
(59) Oldenziel, W. H.; Westerink, B. H. C. Improving Glutamate Microsensors by Optimizing the Composition of the Redox Hydrogel. *Anal. Chem.* **2005**, *77* (17), 5520−5528.
(60) Batra, B.; Pundir, C. S. An Amperometric Glutamate Biosensor Based on Immobilization of Glutamate Oxidase onto Carboxylated Multiwalled Carbon Nanotubes/Gold Nanoparticles/Chitosan Composite Film Modified Au Electrode. *Biosens. Bioelectron.* **2013**, *47*, 496−501.
(61) Frey, O.; van der Wal, P.; de Rooij, N.; Koudelka-Hep, M.In *Development and Characterization of Choline and L-Glutamate Biosensor Integrated on Silicon Microprobes for in-Vivo Monitoring*, Annual International Conference of the IEEE Engineering in Medicine and Biology Society, 2007; pp 6040−6043.
(62) Chen, J.; Yu, Q.; Fu, W.; Chen, X.; Zhang, Q.; Dong, S.; Chen, H.; Zhang, S. A Highly Sensitive Amperometric Glutamate Oxidase Microbiosensor Based on a Reduced Graphene Oxide/Prussian Blue Nanocube/Gold Nanoparticle Composite Film-Modified Pt Electrode. *Sensors* **2020**, *20* (10), 2924.
(63) Meunier, C. J.; Sombers, L. A. Fast-Scan Voltammetry for In Vivo Measurements of Neurochemical Dynamics. In *The Brain Reward System*; Fakhoury, M., Ed.; Springer US: New York, NY, 2021; pp 93−123.
(64) Roberts, J. G.; Lugo-Morales, L. Z.; Loziuk, P. L.; Sombers, L. A. Real-Time Chemical Measurements of Dopamine Release in the Brain. In *Dopamine*; Kabbani, N., Ed.; Methods in Molecular Biology; Humana Press: Totowa, NJ, 2013; Vol. *964*, pp 275−294.
(65) Rice, M. E. H_2O_2: A Dynamic Neuromodulator. *Neuroscientist* **2011**, *17* (4), 389−406.
(66) Chen, B. T.; Avshalumov, M. V.; Rice, M. E. H(2)O(2) Is a Novel, Endogenous Modulator of Synaptic Dopamine Release. *J. Neurophysiol.* **2001**, *85* (6), 2468−2476.
(67) Spanos, M.; Gras-Najjar, J.; Letchworth, J. M.; Sanford, A. L.; Toups, J. V.; Sombers, L. A. Quantitation of Hydrogen Peroxide Fluctuations and Their Modulation of Dopamine Dynamics in the Rat Dorsal Striatum Using Fast-Scan Cyclic Voltammetry. *ACS Chem. Neurosci.* **2013**, *4* (5), 782−789.
(68) Halliwell, B. Oxidative Stress and Neurodegeneration: Where Are We Now? *J. Neurochem.* **2006**, *97* (6), 1634−1658.
(69) Dzubay, J. A.; Jahr, C. E. The Concentration of Synaptically Released Glutamate Outside of the Climbing Fiber-Purkinje Cell Synaptic Cleft. *J. Neurosci.* **1999**, *19* (13), 5265−5274.
(70) Miller, D. R.; McClain, E. S.; Cliffel, D. E. Electrochemical Microphysiometry Detects Cellular Glutamate Uptake. *J. Electrochem. Soc.* **2018**, *165* (12), G3120−G3124.
(71) Mitchell, E. C.; Dunaway, L. E.; McCarty, G. S.; Sombers, L. A. Spectroelectrochemical Characterization of the Dynamic Carbon-Fiber Surface in Response to Electrochemical Conditioning. *Langmuir* **2017**, *33* (32), 7838−7846.

https://doi.org/10.1021/acssensors.3c01267
ACS Sens. 2023, 8, 4091−4100

(72) Venton, B. J.; Michael, D. J.; Wightman, R. M. Correlation of Local Changes in Extracellular Oxygen and pH That Accompany Dopaminergic Terminal Activity in the Rat Caudate-Putamen. *J. Neurochem.* **2003**, *84* (2), 373−381.
(73) Holmes, J.; Witt, C. E.; Keen, D.; Buchanan, A. M.; Batey, L.; Hersey, M.; Hashemi, P. Glutamate Electropolymerization on Carbon Increases Analytical Sensitivity to Dopamine and Serotonin: An Auspicious In Vivo Phenomenon in Mice? *Anal. Chem.* **2021**, *93* (31), 10762−10771.
(74) Heien, M. L. A. V.; Phillips, P. E. M.; Stuber, G. D.; Seipel, A. T.; Wightman, R. M. Overoxidation of Carbon-Fiber Microelectrodes Enhances Dopamine Adsorption and Increases sensitivity. *Analyst* **2003**, *128* (12), 1413.
(75) Schmidt, A. C.; Wang, X.; Zhu, Y.; Sombers, L. A. Carbon Nanotube Yarn Electrodes for Enhanced Detection of Neurotransmitter Dynamics in Live Brain Tissue. *ACS Nano* **2013**, *7* (9), 7864−7873.
(76) Dalangin, R.; Kim, A.; Campbell, R. E. The Role of Amino Acids in Neurotransmission and Fluorescent Tools for Their Detection. *Int. J. Mol. Sci.* **2020**, *21* (17), 6197.
(77) Szerb, J. C.; O'Regan, P. A. Effect of Glutamine on Glutamate Release from Hippocampal Slices Induced by High K^+ or by Electrical Stimulation: Interaction with Different Ca^{2+} Concentrations. *J. Neurochem.* **1985**, *44* (6), 1724−1731.
(78) Whitton, P. S. Glutamatergic Control over Brain Dopamine Release in Vivo and in Vitro. *Neurosci. Biobehav. Rev.* **1997**, *21* (4), 481−488.
(79) Kulagina, N. V.; Zigmond, M. J.; Michael, A. C. Glutamate Regulates the Spontaneous and Evoked Release of Dopamine in the Rat Striatum. *Neuroscience* **2001**, *102* (1), 121−128.
(80) Moghaddam, B.; Gruen, R. J.; Roth, R. H.; Bunney, B. S.; Adams, R. N. Effect of L-Glutamate on the Release of Striatal Dopamine: In Vivo Dialysis and Electrochemical Studies. *Brain Res.* **1990**, *518* (1−2), 55−60.
(81) Westerink, B. H. C.; Santiago, M.; De Vries, J. B. In Vivo Evidence for a Concordant Response of Terminal and Dendritic Dopamine Release during Intranigral Infusion of Drugs. *Naunyn-Schmiedeberg's Arch. Pharmacol.* **1992**, *346* (6), 637−643.
(82) Avshalumov, M. V.; Chen, B. T.; Marshall, S. P.; Peña, D. M.; Rice, M. E. Glutamate-Dependent Inhibition of Dopamine Release in Striatum Is Mediated by a New Diffusible Messenger, H2O2. *J. Neurosci.* **2003**, *23* (7), 2744−2750.

https://doi.org/10.1021/acssensors.3c01267
ACS Sens. 2023, 8, 4091−4100